Journal of King Saud University – Engineering Sciences xxx (xxxx) xxx

Contents lists available at ScienceDirect

Journal of King Saud University – Engineering Sciences

journal homepage: www.sciencedirect.com

Original article

# Augmented hunger games search algorithm using logarithmic spiral opposition-based learning for function optimization and controller design

Davut Izci [a], Serdar Ekinci [b,*], Erdal Eker [c], Murat Kayri [d]

[a] Department of Electronics & Automation, Batman University, Batman 72060 Turkey
[b] Department of Computer Engineering, Batman University, Batman 72100, Turkey
[c] Vocational School of Social Sciences, Mus Alparslan University, Mus, Turkey
[d] Department of Computer and Instructional Technology Education, Van Yuzuncu Yil University, Van, Turkey

ARTICLE INFO

*Article history:*
Received 19 August 2021
Accepted 5 March 2022
Available online xxxx

*Keywords:*
Magnetic ball suspension system
FOPID controller
Hunger games search algorithm
Logarithmic spiral
Opposition-based learning technique

ABSTRACT

This paper explains the construction of a novel augmented hunger games search algorithm using a logarithmic spiral opposition-based learning technique. The proposed algorithm (LsOBL-HGS) is used as an efficient tool for both function optimization and controller design. To assess the performance of the algorithm for function optimization, benchmark functions from the CEC2017 test suite were employed and comparisons were made with available and good performing algorithms. In terms of controller design, the proposed LsOBL-HGS algorithm was utilized to design a FOPID controlled magnetic ball suspension system. Comparative assessments were also performed for FOPID controller design, as well using other state-of-the-art methods reported for the magnetic ball suspension system. The results showed that the proposed LsOBL-HGS algorithm has good capability for FOPID controller design employed in a magnetic ball suspension system as it provided an improvement of more than 13% in terms of the transient response-related parameters and more than 34% in terms of bandwidth compared to the best-reported approach used for comparisons.


## 1. Introduction

Magnetic suspension refers to magnetic-based non-contact lifting which has promising potential for real-world engineering applications, therefore it keeps gaining significant attention amongst researchers. The employment of magnetic-based non-contact lifting can be observed in high-speed trains, vibration isolation, and non-friction bearings. However, an appropriate controller mechanism must be integrated with the magnetic suspension systems as this concept has a nonlinear and unstable structure. Therefore, different controlling mechanisms have so far been reported for this purpose (Acharya et al., 2020; Ahmad et al., 2014; Bauer and Baranowski, 2020; García-Gutiérrez et al., 2019; Mughees and Mohsin, 2020; Sadek et al., 2017). The wider employment of proportional-integral-derivative (PID) controllers can easily be observed amongst the available mechanisms which is due to their relatively easier applicability (Yadav et al., 2016). However, for an increased capability, fractional-order PID (FOPID) controllers are more demanding (Izci and Ekinci, 2021). Because the latter one utilizes fractional terms, it can provide an additional degree of freedom which makes them desirable candidates for dynamic systems (Altbawi et al., 2021; George et al., 2022; Izci et al., 2022b; Kommula and Kota, 2020).

Appropriate tuning schemes for parameter adjustments are required to benefit from the advantages of the aforementioned controllers. In that sense, the metaheuristic algorithms can be employed as unbeatable candidates to tune controllers employed in magnetic ball suspension systems (Roy et al., 2016). Some of the related examples are manta ray foraging optimization (Ekinci et al., 2021), slime mould algorithm (Izci et al., 2021), grey wolf optimization (Ataşlar-Ayyıldız et al., 2021), and particle swarm optimization (Ataşlar-Ayyıldız et al., 2021; Zhang et al., 2021)

* Corresponding author.
*E-mail addresses:* davut.izci@batman.edu.tr (D. Izci), serdar.ekinci@batman.edu.tr (S. Ekinci), e.eker@alparslan.edu.tr (E. Eker), muratkayri@yyu.edu.tr (M. Kayri).
Peer review under responsibility of King Saud University.

Production and hosting by Elsevier

https://doi.org/10.1016/j.jksues.2022.03.001
1018-3639/

Please cite this article as: D. Izci, S. Ekinci, E. Eker et al., Augmented hunger games search algorithm using logarithmic spiral opposition-based learning for function optimization and controller design, Journal of King Saud University – Engineering Sciences, https://doi.org/10.1016/j.jksues.2022.03.001

along with bird swarm algorithm and elephant herding optimization (Dey et al., 2021). Considering the demonstrated promise of those metaheuristic techniques, this paper aims to use an augmented hunger games search (HGS) algorithm (Yang et al., 2021) to tune a FOPID controller for a magnetic ball suspension system to reach better performance compared to previously reported works.

In this study, an opposition-based learning (OBL) technique (Tizhoosh, 2005) was used to enhance the HGS algorithm. The latter technique increases the probability of finding a solution closer to the global optimum. Different examples of OBL versions and their role for performance improvement of the metaheuristic algorithms can be seen in the literature. Some of the recent examples can be listed as shuffled frog-leaping algorithm (Sharma and Pant, 2018), grey wolf optimizer (Long et al., 2019), Harris hawks optimization (Gupta et al., 2020), tunicate swarm algorithm (Sharma et al., 2021) and Lévy flight distribution algorithm (Izci et al., 2022a). Unlike the listed studies, this paper proposes a logarithmic spiral (Mirjalili and Lewis, 2016) version of the OBL technique to enhance the HGS algorithm so that the probability of finding the global optimum increases significantly.

To justify the capability of the augmented HGS using logarithmic spiral opposition-based learning (LsOBL-HGS) algorithm for function optimization, a CEC2017 test suite was employed as it includes challenging benchmark functions for evaluation of the algorithms. The comparative assessment of the proposed LsOBL-HGS algorithm was performed against grey wolf optimization (Mirjalili et al., 2014), Harris hawks optimization (Heidari et al., 2019), and aquila optimization (Abualigah et al., 2021) algorithms as well as the original version of HGS (Yang et al., 2021) algorithm. Then, a FOPID controller was designed based on the proposed LsOBL-HGS algorithm for a magnetic ball suspension system in order to assess the ability of the proposed algorithm for a real-world complex engineering optimization problem. A performance index called *ZLG* (Izci et al., 2022c) was adopted as an objective function to reach the optimal parameters of the FOPID controller. Several comparative assessments were carried out for the latter task using other reported state-of-the-art methods of artificial electric field algorithm based FOPID controller (Demirören et al., 2021), artificial bee colony algorithm based FOPID controller (Demirören et al., 2021), and atom search optimization based FOPID controller (Demirören et al., 2021). All the analyses related to function optimization and the controller design for the magnetic ball suspension system showed superior capability of the proposed LsOBL-HGS algorithm for different optimization problems.

## 2. Hunger games search algorithm

The animals' instinct to survive has motivated the development of the HGS algorithm (Yang et al., 2021). The hunger-driven activities and behavioral choices amongst the animals are considered as a set of game rules by the HGS algorithm. During foraging, social animals mainly cooperate; however, few individuals may not take part. Such a cooperative communication and foraging behavior is represented by Eq. (1):

$$\overrightarrow{X(t+1)} = \begin{cases} Game_1 : \overrightarrow{X(t)} \cdot (1 + randn(1)), r_1 < l \\ Game_2 : \overrightarrow{W_1} \cdot \overrightarrow{X_b} + \vec{R} \cdot \overrightarrow{W_2} \cdot \left| \overrightarrow{X_b} - \overrightarrow{X(t)} \right|, r_1 > l, r_2 > E \\ Game_3 : \overrightarrow{W_1} \cdot \overrightarrow{X_b} - \vec{R} \cdot \overrightarrow{W_2} \cdot \left| \overrightarrow{X_b} - \overrightarrow{X(t)} \right|, r_1 > l, r_2 < E \end{cases} \quad (1)$$

where two random numbers, within the range of $[0, 1]$, are denoted by $r_1$ and $r_2$; the current iteration is shown by $t$ , and a random number satisfying normal distribution is represented by $randn(1)$. The hunger weights are denoted by $W_1$ and $W_2$. The locations of each agent and the best agent are represented by $X(t)$ and $X_b$, respectively, for the current iteration. The parameter of $l$ helps improve the algorithm. $R$ represents a number, within $[-\alpha, \alpha]$, which is calculated as follows:

$$\vec{R} = 2 \times shrink \times rand - shrink \quad (2)$$

where $shrink = 2 \times (1 - \frac{t}{T})$, $rand$ is a random number within $[0, 1]$ and $T$ is the maximum number of iterations. The parameter of $E$, given in Eq. (1), stands for a variation control for all positions and is defined as:

$$E = sech(|F(i) - BF|), i \in 1, 2, \cdots, n \quad (3)$$

where $F(i)$ and $BF$ are the fitness value of each agent and the best fitness value, respectively, obtained so far. The hyperbolic function of *sech* is defined as $2/(e^x + e^{-x})$. The starvation characteristics of the individuals are mathematically simulated by the hunger weights which are defined in Eqs. (4) and (5):

$$\overrightarrow{W_1(i)} = \begin{cases} hng(i) \cdot \frac{N}{Shng} \times r_4, r_3 < l \\ 1, r_3 > l \end{cases} \quad (4)$$

$$\overrightarrow{W_2(i)} = (1 - e^{-|hng(i) - Shng|}) \times r_5 \times 2 \quad (5)$$

where $N$ denotes the number of individuals and $hng$ is the hunger for individuals. Besides, $r_3$, $r_4$ and $r_5$ are all random numbers within the range of $[0, 1]$, and $Shng$ denotes the sum of hungry feelings of all individuals. The parameter of $hng(i)$ is defined as follows:

$$hng(i) = \begin{cases} 0, Allfit(i) == BF \\ hng(i) + H, Allfit(i) ! = BF \end{cases} \quad (6)$$

where $Allfit(i)$ holds the fitness of each agent in the current iteration and $BF$ stands for the best fitness obtained so far.

The term of $H$ denotes hunger sensation which is calculated as follows:

$$H = \begin{cases} LH \times (1 + r), TH < LH \\ TH, TH \geq LH \end{cases} \quad (7)$$

where $TH = (F(i) - BF/(WF - BF)) \times r_6 \times 2 \times (UB - LB)$. In the above equation, $LH$ stands for the lower bound whereas $UB$ and $LB$ are the feature space-related upper and lower bounds, respectively. $F(i)$ represents the fitness value of each agent and $WF$ denotes the worst fitness value obtained so far. Fig. 1 represents the logic of the HGS algorithm for the optimization tasks.

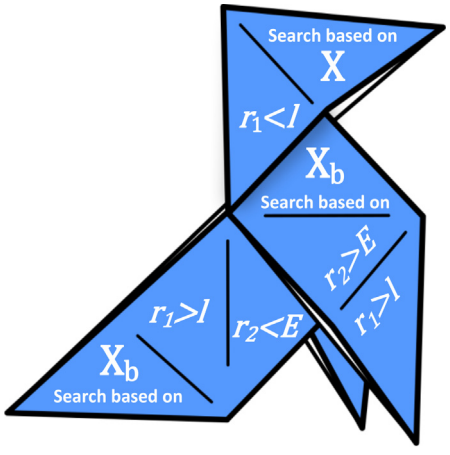


**Fig. 1.** The logic of the HGS algorithm (Yang et al., 2021).

**Table 1**
Statistical results of CEC2017 benchmark functions.

| Function ID | Index | LsOBL-HGS | HGS | GWO | HHO | AO |
|---|---|---|---|---|---|---|
| F1 | Mean | 6.3653E + 03 | 7.0169E + 03 | 4.0610E + 06 | 3.2043E + 05 | 5.2861E + 05 |
| | Std | 4.3602E + 03 | 4.5034E + 03 | 1.1985E + 07 | 1.7349E + 05 | 3.7558E + 05 |
| F3 | Mean | 3.0000E + 02 | 3.0407E + 02 | 1.3305E + 03 | 3.0194E + 02 | 4.3646E + 02 |
| | Std | 3.7683E − 04 | 4.1351E − 01 | 1.4570E + 03 | 8.2897E − 01 | 1.2893E + 02 |
| F4 | Mean | 4.0215E + 02 | 4.1629E + 02 | 4.1654E + 02 | 4.1373E + 02 | 4.0906E + 02 |
| | Std | 1.6369E + 00 | 1.7549E + 01 | 1.1913E + 01 | 2.6009E + 01 | 2.6773E + 00 |
| F5 | Mean | 5.1301E + 02 | 5.3111E + 02 | 5.1662E + 02 | 5.4745E + 02 | 5.3048E + 02 |
| | Std | 6.2533E + 00 | 8.2482E + 00 | 7.9230E + 00 | 1.6628E + 01 | 1.0244E + 01 |
| F6 | Mean | 6.0047E + 02 | 6.0086E + 02 | 6.0112E + 02 | 6.3386E + 02 | 6.1767E + 02 |
| | Std | 4.9390E − 01 | 5.8827E − 01 | 1.1589E + 00 | 9.4315E + 00 | 7.4753E + 00 |
| F7 | Mean | 7.2426E + 02 | 7.3922E + 02 | 7.3146E + 02 | 7.7836E + 02 | 7.4321E + 02 |
| | Std | 1.0510E + 01 | 1.0563E + 01 | 1.5206E + 01 | 1.6991E + 01 | 1.2803E + 01 |
| F8 | Mean | 8.0797E + 02 | 8.1952E + 02 | 8.1523E + 02 | 8.3397E + 02 | 8.2138E + 02 |
| | Std | 4.4509E + 00 | 6.7994E + 00 | 5.4020E + 00 | 7.3463E + 00 | 8.1810E + 00 |
| F9 | Mean | 9.0003E + 02 | 9.0076E + 02 | 9.0889E + 02 | 1.3815E + 03 | 9.8064E + 02 |
| | Std | 1.2256E − 01 | 2.6252E + 00 | 1.6225E + 01 | 2.3865E + 02 | 1.1529E + 02 |
| F10 | Mean | 1.4293E + 03 | 1.6081E + 03 | 1.5204E + 03 | 2.0521E + 03 | 1.7943E + 03 |
| | Std | 2.0268E + 02 | 2.8205E + 02 | 2.2130E + 02 | 3.7043E + 02 | 2.4160E + 02 |
| F11 | Mean | 1.1260E + 03 | 1.1426E + 03 | 1.1461E + 03 | 1.1706E + 03 | 1.1837E + 03 |
| | Std | 2.0199E + 01 | 4.5226E + 01 | 6.4788E + 01 | 4.8788E + 01 | 4.8085E + 01 |
| F12 | Mean | 8.3420E + 03 | 2.0088E + 04 | 7.6224E + 05 | 2.9705E + 06 | 3.7110E + 06 |
| | Std | 3.8655E + 03 | 2.0504E + 04 | 7.8042E + 05 | 2.9031E + 06 | 3.8531E + 06 |
| F13 | Mean | 5.7306E + 03 | 1.1601E + 04 | 1.2213E + 04 | 1.8435E + 04 | 1.8428E + 04 |
| | Std | 5.0020E + 03 | 6.7794E + 03 | 9.5275E + 03 | 1.2193E + 04 | 1.4134E + 04 |
| F14 | Mean | 1.4674E + 03 | 2.5539E + 03 | 2.9096E + 03 | 1.6381E + 03 | 1.8429E + 03 |
| | Std | 5.4467E + 01 | 1.6348E + 03 | 1.8624E + 03 | 1.4231E + 02 | 2.9225E + 02 |
| F15 | Mean | 3.1890E + 03 | 4.2862E + 03 | 4.9329E + 03 | 4.9655E + 03 | 4.4719E + 03 |
| | Std | 2.9484E + 03 | 2.7760E + 03 | 1.7729E + 03 | 1.3857E + 03 | 1.6239E + 03 |
| F16 | Mean | 1.7352E + 03 | 1.7595E + 03 | 1.7807E + 03 | 1.8054E + 03 | 1.7678E + 03 |
| | Std | 1.0251E + 02 | 1.3625E + 02 | 1.2253E + 02 | 1.4939E + 02 | 1.2409E + 02 |
| F17 | Mean | 1.7181E + 03 | 1.7605E + 03 | 1.8206E + 03 | 1.7663E + 03 | 1.7758E + 03 |
| | Std | 2.1152E + 01 | 4.6985E + 01 | 4.3391E + 01 | 3.3727E + 01 | 2.2756E + 01 |
| F18 | Mean | 2.0802E + 04 | 2.3978E + 04 | 3.1449E + 04 | 1.6759E + 04 | 2.5521E + 04 |
| | Std | 1.1300E + 04 | 1.4398E + 04 | 1.5085E + 04 | 1.2793E + 04 | 1.4708E + 04 |
| F19 | Mean | 3.3399E + 03 | 1.1699E + 04 | 6.3225E + 03 | 9.7714E + 03 | 6.3080E + 03 |
| | Std | 1.9350E + 03 | 1.1134E + 04 | 5.8568E + 03 | 8.1075E + 03 | 5.7503E + 03 |
| F20 | Mean | 2.0127E + 03 | 2.0216E + 03 | 2.1210E + 03 | 2.1687E + 03 | 2.1175E + 03 |
| | Std | 9.3435E + 00 | 1.1342E + 01 | 4.7479E + 01 | 7.7306E + 01 | 5.6107E + 01 |
| F21 | Mean | 2.2190E + 03 | 2.3710E + 03 | 2.3170E + 03 | 2.3097E + 03 | 2.2906E + 03 |
| | Std | 3.2251E + 01 | 3.3974E + 01 | 6.6931E + 00 | 5.9256E + 01 | 5.7181E + 01 |
| F22 | Mean | 2.2626E + 03 | 2.3131E + 03 | 2.3486E + 03 | 2.4552E + 03 | 2.3008E + 03 |
| | Std | 1.7262E + 01 | 1.0733E + 02 | 3.0446E + 01 | 2.4480E + 02 | 8.9167E + 00 |
| F23 | Mean | 2.6158E + 03 | 2.6239E + 03 | 2.6228E + 03 | 2.6869E + 03 | 2.6470E + 03 |
| | Std | 5.6411E + 00 | 6.4239E + 00 | 8.3269E + 00 | 2.4361E + 01 | 1.4580E + 01 |
| F24 | Mean | 2.6042E + 03 | 2.7792E + 03 | 2.7439E + 03 | 2.7155E + 03 | 2.7356E + 03 |
| | Std | 8.9321E + 01 | 1.2627E + 01 | 1.4595E + 01 | 1.1826E + 02 | 7.1265E + 01 |
| F25 | Mean | 2.9194E + 03 | 2.9329E + 03 | 2.9484E + 03 | 2.9408E + 03 | 2.9161E + 03 |
| | Std | 3.1642E + 01 | 3.3730E + 01 | 2.3786E + 01 | 2.1743E + 01 | 2.1498E + 01 |
| F26 | Mean | 2.9645E + 03 | 3.2376E + 03 | 2.9886E + 03 | 3.3700E + 03 | 2.9356E + 03 |
| | Std | 2.1066E + 02 | 4.3722E + 02 | 3.1668E + 02 | 4.6435E + 02 | 1.5733E + 02 |
| F27 | Mean | 3.0878E + 03 | 3.0958E + 03 | 3.1274E + 03 | 3.1807E + 03 | 3.1038E + 03 |
| | Std | 2.2515E + 00 | 1.7410E + 01 | 1.8878E + 01 | 5.1694E + 01 | 4.1658E + 00 |
| F28 | Mean | 3.2208E + 03 | 3.2559E + 03 | 3.3622E + 03 | 3.3503E + 03 | 3.3917E + 03 |
| | Std | 1.2620E + 02 | 1.4485E + 02 | 1.0235E + 02 | 1.5171E + 02 | 1.0682E + 02 |
| F29 | Mean | 3.1747E + 03 | 3.2371E + 03 | 3.2124E + 03 | 3.3541E + 03 | 3.2417E + 03 |
| | Std | 3.2944E + 01 | 5.6416E + 01 | 7.4610E + 01 | 1.2806E + 02 | 5.7123E + 01 |
| F30 | Mean | 1.9927E + 05 | 3.5948E + 05 | 5.6525E + 05 | 1.3405E + 06 | 4.1545E + 05 |
| | Std | 3.6602E + 05 | 5.4532E + 05 | 6.7458E + 05 | 1.5193E + 06 | 5.3863E + 05 |

## 3. Proposed novel LsOBL-HGS algorithm

The OBL strategy is capable of enhancing the exploration of the algorithms since it provides the opportunity of avoiding local stagnation (Izci et al., 2020). The OBL mechanism can be explained as $X_{op} = UB + LB - X$ where $X$ is a real number within boundaries of $[LB, UB]$ and $X_{op}$ is the opposite of that number. In the OBL, $X$ and $X_{op}$ are considered together and the best $N$ solutions are selected from their union.

In this study, an augmented HGS algorithm is proposed using a logarithmic spiral OBL (LsOBL) technique. The HGS algorithm firstly finds the optimal position so far ($X_{\text{best}}$). Then the opposite position of $X_{op}$ is obtained with the modified OBL technique using the following form:

$$X_{op} = \varphi_1 \cdot UB + \varphi_2 \cdot LB - X_{best} \tag{8}$$

where $\varphi_1$ and $\varphi_2$ are random numbers within (0,1) and updated in each iteration. In this way, the opposite solution is built, and the unpredictability of the exploration is increased. After this step, a dynamic logarithmic spiral space between modified $X_{op}$ and $X_{best}$ is constructed in each iteration using the following description:

$$X_{t+1} = \left|X_{best} - X_{op}\right| \times e^{bl} \times \cos(2\pi l) + X_{best} \tag{9}$$

where $X_{t+1}$ is the position vector of $X$ at the moment of $t+1$, $l$ is a random value within $[-1, 1]$ and determines how much the $X_{t+1}$ is close to the $X_{best}$ whereas a spiral shape is constructed for $b = 1$. Once the above definition is completed, random exploration is performed by the proposed algorithm as the last step. It is worth noting that the value of $l$ has a significant role as it controls the exploration activities of the search agents for the entire logarithmic spiral space since $l = -1$ means the agent is within the closest position to the $X_{best}$ whereas the farthest position is indicated by $l = 1$. Considering this significance, each of the agents of the HGS algorithm was assigned different $l$ values in each iteration using the definition of $l = 2 \times rand - 1$ where $rand$ denotes a random number within $(0, 1)$.

The proposed algorithm provides the following advantages. Firstly, it reduces the exploration space significantly as the constructed logarithmic spiral space is smaller than the entire exploration space. Secondly, more promising regions are considered for performing the exploration compared to the OBL scheme. Therefore, the proposed LsOBL-HGS algorithm maintains the diversity of exploration areas within a limited time and prevents the early convergence of the original form of the HGS algorithm.

## 4. Experimental results on recent benchmark functions

### 4.1. CEC2017 benchmark functions and compared algorithms

Twenty-nine benchmark functions from the CEC2017 test suite (Awad et al., 2016) were used for this study in order to perform the initial statistical assessment. Those benchmark functions provide a good platform for the performance assessment of the algorithms as they are challenging problems. In terms of comparative evaluation, the performance of the proposed LsOBL-HGS algorithm was assessed against other metaheuristic algorithms of grey wolf optimizer (GWO) (Mirjalili et al., 2014) as it is one of the most cited metaheuristic algorithms, along with Harris hawks optimization (HHO) (Heidari et al., 2019) and Aquila optimizer (AO) (Abualigah et al., 2021) algorithms as the latter ones are the recently reported and competitive algorithms. Besides, the original version of the HGS (Yang et al., 2021) algorithm was also used for making comparisons. All the algorithms were used with their default parameter values along with a population size of 50 and a total iteration number of 1,000. In addition, all the algorithms were run 30 times.

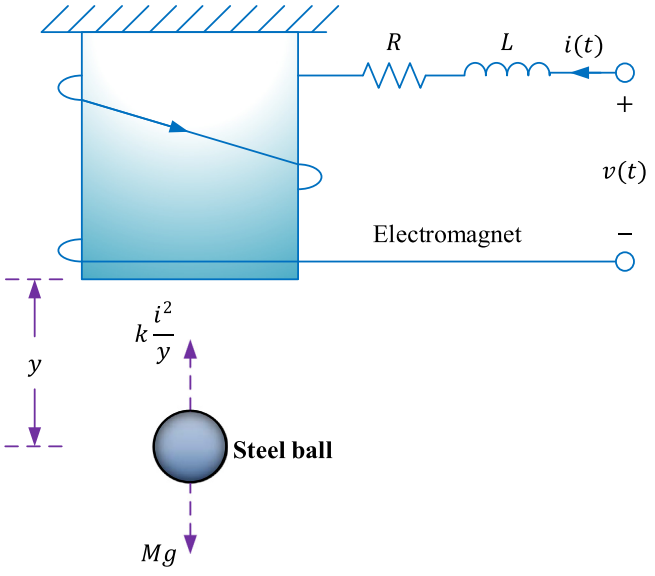


**Fig. 2.** Representation of magnetic ball suspension system.

### 4.2. Statistical performance

The CEC2017 test suite includes both unimodal (F01, F03) and multimodal (F04 - F10) functions which are good tools to assess the exploitation and exploration abilities of the algorithms. Apart from the latter forms, the CEC2017 test suite also includes hybrid (F11 – F20) and composition (F21 – F30) functions which are more challenging for test functions. Table 1 lists the comparative results on those functions in terms of the statistical performance criteria of mean and standard deviation (Std). The numerical values in Table 1 clearly show that the proposed LsOBL-HGS has better statistical performance than the compared ones.

## 5. Mathematical modeling of magnetic ball suspension system

The changing current passing through the coil of an electromagnet causes the field strength to change which makes the suspension of a ferromagnetic ball feasible. Fig. 2 provides a schematic representation of such a system. However, it is not easy to control this system because of its nonlinear and unstable nature. A feedback control system can be employed to address the latter issue, considering the dynamic behavior of the system.

The following Eq. (10) defines the net force acting on the ball (Golnaraghi and Kuo, 2017) where $k$, $g$, and $M$ denote the electromagnet coefficient, the gravitational acceleration, and the mass of the ball, respectively.

$$M\frac{d^2y(t)}{dt^2} = M \cdot g - k\frac{i^2(t)}{y(t)} \tag{10}$$

In the latter definition, $y(t)$ stands for the position of the ball. The input voltage, $v(t)$ and the current, $i(t)$ of the coil can be explained with the following form where $R$ and $L$ denote the winding resistance and inductance, respectively.

$$v(t) = R \cdot i(t) + L\frac{di(t)}{dt} \tag{11}$$

The following linearized set of equations can be obtained where $A^*$ and $B^*$ are the coefficient matrices as shown in Eq. (12) (Golnaraghi and Kuo, 2017):

$$A^* = \begin{bmatrix} 0 & 1 & 0 \\ \frac{g}{x_{10}} & 0 & -2\sqrt{\frac{k \cdot g}{M \cdot x_{10}}} \\ 0 & 0 & -\frac{R}{L} \end{bmatrix}, B^* = \begin{bmatrix} 0 \\ 0 \\ 1/L \end{bmatrix} \tag{12}$$

Table 2 lists the parameters and the corresponding values of the magnetic ball suspension system which is considered in the present paper (Golnaraghi and Kuo, 2017).

### 5.1. Analysis of the system without a controller

The following transfer function can be obtained for the magnetic ball suspension system by adopting the related values for the listed parameters given in Table 2 and considering the equilibrium point of $y_0(t) = 0.5m$.

$$G(s) = C^*(sI - A^*)^{-1}B^* = [1 \quad 0 \quad 0](sI - A^*)^{-1}B^* = -\frac{885.9}{s^3 + 100s^2 - 19.62s - 1962} \tag{13}$$

The pole/zero map and the open-loop step response of the system, provided in Fig. 3, can be obtained using Eq. (13). One of the poles of the system is located in the right half-plane; it implies the unstable nature of the system which is also confirmed with the open-loop response of the system.

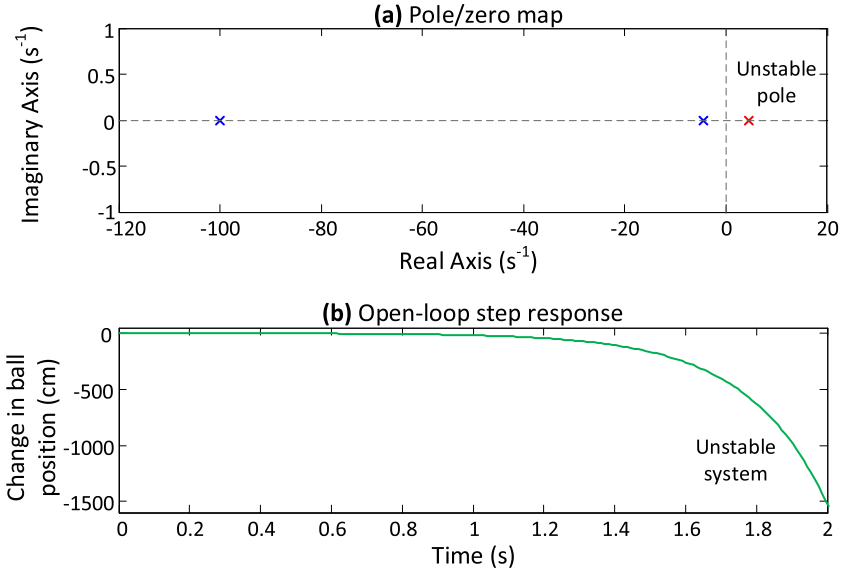


**Fig. 3.** Pole/zero map and open-loop step response of the system.

### 5.2. FOPID controller and its application to the system

Due to the availability of the fractional orders of $\lambda$ and $\mu$, a FOPID controller is a more advanced version of a PID controller and can provide more capability than that of a PID controller. The transfer function of a FOPID controller is defined as follows (Ekinci et al., 2020):

$$G_{FOPID}(s) = K_p + \frac{K_i}{s^{\lambda}} + K_d s^{\mu} \tag{14}$$

where $K_p$, $K_i$, $K_d$, $\lambda$, and $\mu$ are proportional gain, integral gain, derivative gain, fractional integral order, and fractional derivative order, respectively. Fig. 4 illustrates the block diagram of a FOPID controlled magnetic ball suspension system.

The closed-loop transfer function provided in Eq. (15) can be obtained for the magnetic ball suspension system by using the block diagram given above in Fig. 4.

**Table 2**
The system parameters and their values.

| Parameter | Value |
|---|---|
| $R$(Winding resistance) | 1 Ω |
| $M$(Ball mass) | 1 kg |
| $k$(Proportional constant) | 1 kg-m$^2$/A$^2$-s$^2$ |
| $L$(Winding inductance) | 0.01$H$ |
| $g$(Gravitational acceleration) | 9.81 m/s$^2$ |

$$CLTF(s) = \frac{G_{FOPID}(s)\cdot G(s)}{1 + G_{FOPID}(s)\cdot G(s)} = \frac{-885.9(K_d s^{\lambda+\mu} + K_p s^{\lambda} + K_i)}{(s^3 + 100s^2 - 19.62s - 1962)s^{\lambda} - 885.9(K_d s^{\lambda+\mu} + K_p s^{\lambda} + K_i)} \tag{15}$$

## 6. Problem definition and application of proposed LsOBL-HGS algorithm to the magnetic ball suspension system

The objective function, $ZLG$ (Izci et al., 2022c), was adopted in this paper as the performance index since it is widely employed. This objective function is given with the following form where $e_{ss}$ is the steady-state error, $\%OS$ is the percent overshoot, $t_r$ is the rise time and $t_s$ is the settling time.

$$F = (1 - e^{-\varphi}) \times \left(\frac{\%OS}{100} + e_{ss}\right) + e^{-\varphi} \times (t_s - t_r) \tag{16}$$

$\varphi$, the weighting parameter, was set to 1 (Ekinci et al., 2020) for this study. The block diagram provided in Fig. 5 illustrates the implementation of the proposed LsOBL-HGS algorithm to tune the FOPID controlled magnetic ball suspension system. The population size was chosen as 25 whereas the total iteration number ($t_{max}$) as 50. The algorithm performed the optimization for 30 runs. Apart from the latter values, the limits for the parameters of the FOPID controller were chosen as $-100 \le K_p, K_i, K_d \le 0$ and $0 < \lambda, \mu < 2$ (Demirören et al., 2021) for this study. Meanwhile, the controller parameters may be within negative values for some physical systems (Demirören et al., 2021) as is the case here.

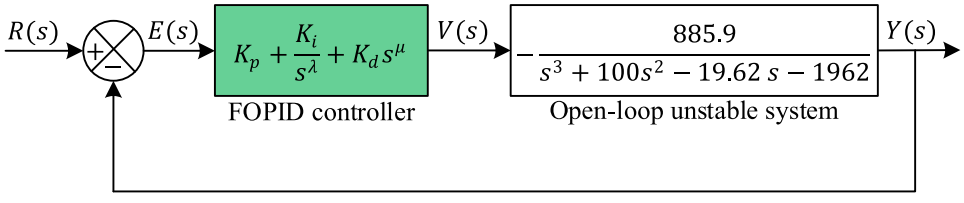


**Fig. 4.** Block diagram of the FOPID controlled system.

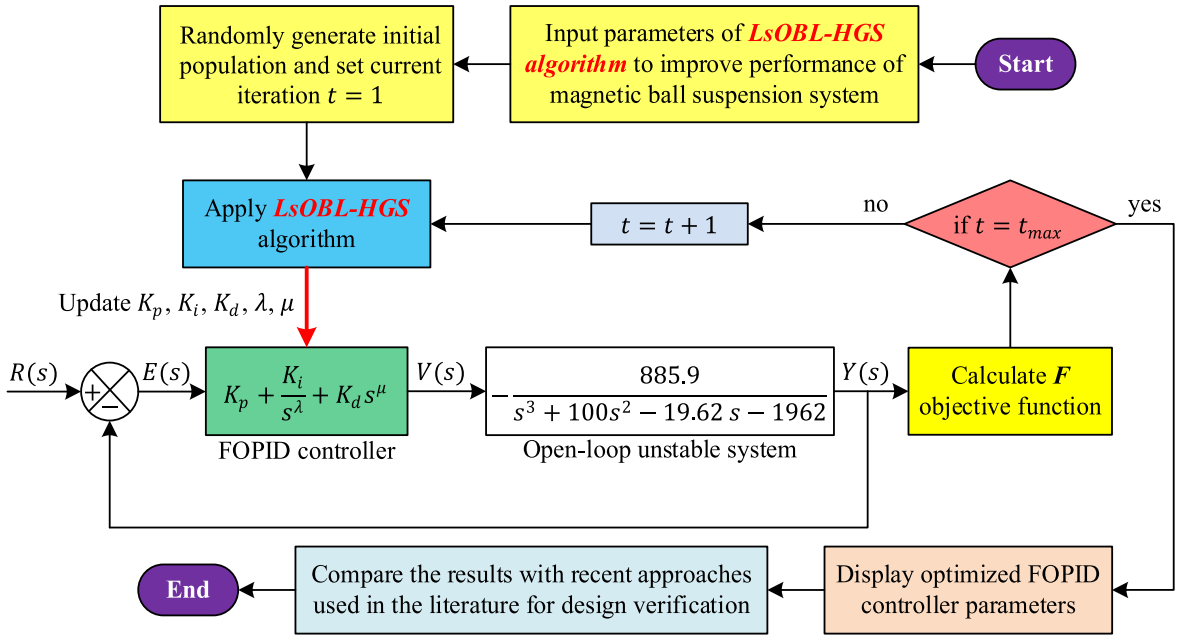


**Fig. 5.** Design of LsOBL-HGS based FOPID controller for the system.

## 7. Comparison with recently reported methods

### 7.1. Compared algorithms and their transfer functions

The performance of the LsOBL-HGS algorithm based FOPID controller for magnetic ball suspension was assessed comparatively using existing methods of artificial electric field algorithm based FOPID controller (AEF/FOPID) (Demirören et al., 2021), artificial bee colony algorithm based FOPID (ABC/FOPID) (Demirören et al., 2021), and atom search optimization based FOPID controller (ASO/FOPID) (Demirören et al., 2021). Table 3 lists those algorithms and the best-obtained values for the gain parameters and fractional orders of the FOPID controller.

Substituting those parameters into Eq. (15) would yield the closed-loop transfer functions (*CLTF*) of the magnetic ball suspension system given in Eqs. (17) - (21) for LsOBL-HGS, HGS, AEF, ASO, and ABC algorithms based FOPID controllers, respectively.

### 7.2. Transient response

The transient response-related performance indicators are demonstrated in Table 4. Besides, Fig. 6 provides the illustrative step responses of the LsOBL-HGS, HGS, AEF, ASO, and ABC algorithms based on FOPID controllers. The provided numerical and illustrative results show that the proposed LsOBL-HGS algorithm-based FOPID controller reaches less values of the related performance indicators, thus, clearly indicating a better time response profile of the proposed LsOBL-HGS algorithm based FOPID controller for the magnetic ball suspension system.

### 7.3. Frequency response

The numerical values for the frequency response-related performance indicators are listed in Table 5 for LsOBL-HGS, HGS, AEF, ASO, and ABC algorithms based FOPID controllers. Besides, Fig. 7

$$CLTF_{LsOBL-HGS}(s) = \frac{2795.5s^{2.1074} + 87557s^{0.8175} + 67283}{s^{3.8175} + 100s^{2.8175} + 2795.5s^{2.1074} - 19.62s^{1.8175} + 85595s^{0.8175} + 67283} \quad (17)$$

$$CLTF_{HGS}(s) = \frac{2194.2s^{2.2485} + 74027s^{0.9202} + 73038}{s^{3.9202} + 100s^{2.9202} + 2194.2s^{2.2485} - 19.62s^{1.9202} + 72065s^{0.9202} + 73038} \quad (18)$$

$$CLTF_{AEF}(s) = \frac{3201.5s^{2.1308} + 64547s^{0.9812} + 71783}{s^{3.9812} + 100s^{2.9812} + 3201.5s^{2.1308} - 19.62s^{1.9812} + 62585s^{0.9812} + 71783} \quad (19)$$

$$CLTF_{ASO}(s) = \frac{2406.6s^{2.0443} + 43853s^{0.8845} + 61973}{s^{3.8845} + 100s^{2.8845} + 2406.6s^{2.0443} - 19.62s^{1.8845} + 41891s^{0.8845} + 61973} \quad (20)$$

**Table 3**
Obtained FOPID controller parameters.

| Parameter | LsOBL-HGS | HGS | AEF | ASO | ABC |
|---|---|---|---|---|---|
| $K_p$ | −98.8349 | −83.5623 | −72.8609 | −49.5017 | −83.7975 |
| $K_i$ | −75.9496 | −82.4457 | −81.0298 | −69.9558 | −77.3375 |
| $K_d$ | −3.1556 | −2.4768 | −3.6139 | −2.7166 | −5.0983 |
| $\lambda$ | 0.8175 | 0.9202 | 0.9812 | 0.8845 | 0.9905 |
| $\mu$ | 1.2899 | 1.3283 | 1.1496 | 1.1598 | 1.0293 |

**Table 4**
Comparison of percent overshoot, rise time and settling time.

| Performance indicator | LsOBL-HGS | HGS | AEF | ASO | ABC |
|---|---|---|---|---|---|
| Overshoot (%) | 12.7854 | 14.7983 | 17.1741 | 21.1222 | 27.8227 |
| Rise time (s) | 0.0208 | 0.0244 | 0.0257 | 0.0328 | 0.0246 |
| Settling time (s) | 0.2849 | 0.3087 | 0.3300 | 0.3562 | 0.3448 |

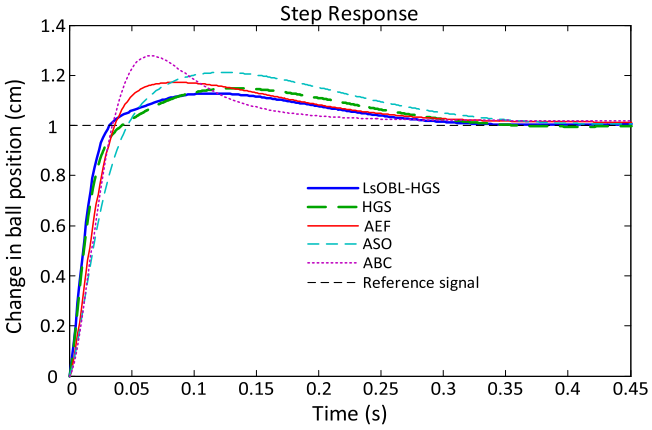


**Fig. 6.** Comparison of step responses.

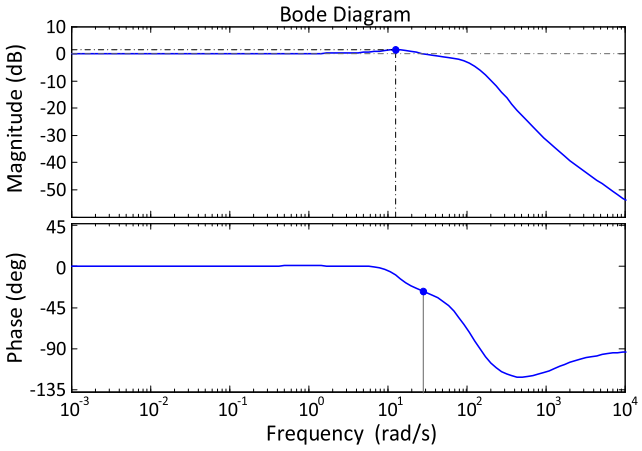


**Fig. 7.** Bode diagram of LsOBL-HGS based FOPID controlled system.

shows the Bode plot of the FOPID controlled magnetic ball suspension system tuned by the LsOBL-HGS algorithm. The comparative numerical results show that the LsOBL-HGS algorithm-based FOPID controller provides the most stable behavior for a magnetic ball suspension system in terms of frequency response.

### 7.4. Effect of the noise signal

The performance of the proposed LsOBL-HGS algorithm-based FOPID controller was also comparatively assessed in terms of suppressing the effect of the noise signal. White Gaussian noise with an input signal power of $1W$ and signal-to-noise ratio (SNR) of $20dB$ was introduced as the measurement noise. Fig. 8 demonstrates the obtained comparative results in this regard. The proposed LsOBL-HGS algorithm-based FOPID controller provides the most optimal dynamic response and deals with the noise better compared to other compared algorithms for the magnetic ball suspension system as can be observed from the respective figures.

### 7.5. Robustness

Lastly, the parameters of $R$ and $L$ were separately changed within ranges of $\pm 5\%$ and $\pm 20\%$, respectively, in order to demonstrate the robustness of the proposed LsOBL-HGS algorithm based FOPID controlled magnetic ball suspension system comparatively. Table 6 provides the comparative results for FOPID controlled magnetic ball suspension systems designed by LsOBL-HGS, HGS, AEF, ASO, and ABC algorithms. From the demonstrated parametric uncertainties, the better ability of the proposed LsOBL-HGS algorithm can be clearly observed.

**Table 5**
Comparison of gain margin, phase margin, and bandwidth.

| Performance indicator | LsOBL-HGS | HGS | AEF | ASO | ABC |
|---|---|---|---|---|---|
| Gain margin (dB) | Inf. | Inf. | Inf. | Inf. | Inf. |
| Phase margin (deg) | 152.7340 | 152.1233 | 133.2568 | 134.5349 | 103.2657 |
| Bandwidth (Hz) | 99.4241 | 83.8238 | 73.7792 | 54.6252 | 75.3558 |

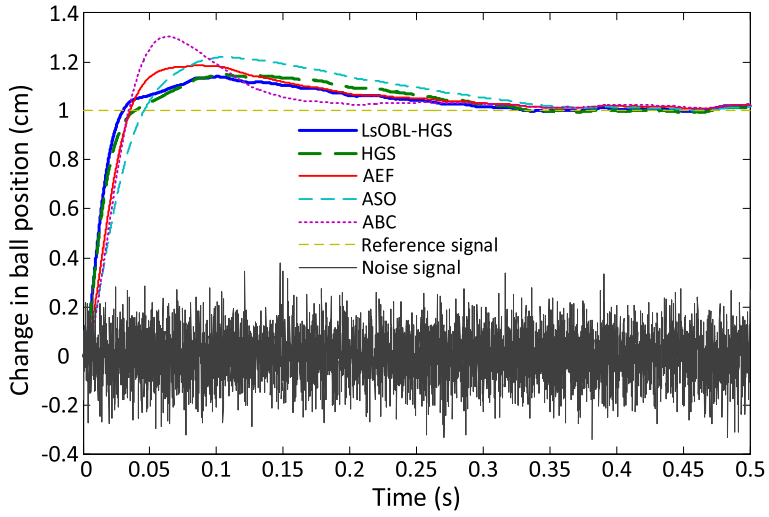


**Fig. 8.** Comparison of step responses in the case of measurement noise.

**Table 6**
Comparison of step responses under parameter uncertainties.

| Parameter changes | Performance indicator | LsOBL-HGS | HGS | AEF | ASO | ABC |
|---|---|---|---|---|---|---|
| $R = 0.95$ | Overshoot (%) | 12.2011 | 14.1220 | 16.6556 | 20.2793 | 28.4027 |
| | Rise time (s) | 0.0198 | 0.0230 | 0.0455 | 0.0313 | 0.0411 |
| | Settling time (s) | 0.2804 | 0.3042 | 0.3272 | 0.3518 | 0.3225 |
| $R = 1.05$ | Overshoot (%) | 13.3684 | 15.4708 | 15.7177 | 21.9624 | 27.2311 |
| | Rise time (s) | 0.0218 | 0.0260 | 0.0458 | 0.0343 | 0.0255 |
| | Settling time (s) | 0.2891 | 0.3129 | 0.3387 | 0.3604 | 0.3866 |
| $L = 0.008$ | Overshoot (%) | 12.5253 | 14.5220 | 16.2963 | 20.4661 | 24.0178 |
| | Rise time (s) | 0.0210 | 0.0257 | 0.0258 | 0.0335 | 0.0244 |
| | Settling time (s) | 0.2886 | 0.3124 | 0.3346 | 0.3615 | 0.3416 |
| $L = 0.012$ | Overshoot (%) | 13.0704 | 15.1044 | 19.1864 | 21.0597 | 31.9315 |
| | Rise time (s) | 0.0210 | 0.0242 | 0.0259 | 0.0486 | 0.0251 |
| | Settling time (s) | 0.2810 | 0.3048 | 0.3252 | 0.3516 | 0.3472 |

## 8. Conclusion

The construction of a novel augmented HGS algorithm using a logarithmic spiral OBL scheme has been discussed in this paper. The novel LsOBL-HGS algorithm has been proposed as an efficient tool both for function optimization and FOPID controller design for the magnetic ball suspension system. Evaluations against benchmark functions from the CEC2017 test suite have shown an increased performance of the proposed LsOBL-HGS algorithm compared to the original form of HGS, GWO, HHO, and AO algorithms. Similarly, the comparative performance of the proposed LsOBL-HGS based FOPID controlled magnetic ball suspension system has been demonstrated using several analyses. The proposed system has demonstrated better performance compared to other state-of-the-art methods of AEF, ASO, and ABC algorithms based FOPID controllers reported for magnetic ball suspension system as the transient response-related parameters have been improved by then 13% and the bandwidth by more than 34% compared to the best-reported approach used for comparisons.

## Declaration of Competing Interest

The authors declare that they have no known competing financial interests or personal relationships that could have appeared to influence the work reported in this paper.

## References

Abualigah, L., Yousri, D., Abd Elaziz, M., Ewees, A.A., Al-qaness, M.A.A., Gandomi, A. H., 2021. Aquila optimizer: A novel meta-heuristic optimization algorithm. Comput. Ind. Eng. 157,. https://doi.org/10.1016/j.cie.2021.107250 107250.

Acharya, D.S., Swain, S.K., Mishra, S.K., 2020. Real-time implementation of a stable 2 DOF PID controller for unstable second-order magnetic levitation system with time delay. Arab. J. Sci. Eng. 45, 6311–6329. https://doi.org/10.1007/s13369-020-04425-6.

Ahmad, I., Shahzad, M., Palensky, P., 2014. Optimal PID control of magnetic levitation system using genetic algorithm. In: 2014 IEEE International Energy Conference (ENERGYCON). IEEE, pp. 1429–1433. 10.1109/ENERGYCON.2014.6850610.

Altbawi, S.M.A., Mokhtar, A.S.B., Jumani, T.A., Khan, I., Hamadneh, N.N., Khan, A., 2021. Optimal design of Fractional order PID controller based Automatic voltage regulator system using gradient-based optimization algorithm. J. King Saud Univ. - Eng. Sci.. https://doi.org/10.1016/j.jksues.2021.07.009.

Ataşlar-Ayyıldız, B., Karahan, O., Yılmaz, S., 2021. Control and robust stabilization at unstable equilibrium by fractional controller for magnetic levitation systems. Fractal Fract. 5, 101. https://doi.org/10.3390/fractalfract5030101.

Awad, N.H., Ali, M.Z., Liang, J., Qu, B.Y., Suganthan, P.N., 2016. Problem definitions and evaluation criteria for the CEC 2017 special session and competition on real-parameter optimization. Nanyang Technol. Univ., Singapore, Tech. Rep 1–34..

Bauer, W., Baranowski, J., 2020. Fractional PIλD Controller Design for a Magnetic Levitation System. Electronics 9, 2135. https://doi.org/10.3390/electronics9122135.

Demirören, A., Ekinci, S., Hekimoğlu, B., Izci, D., 2021. Opposition-based artificial electric field algorithm and its application to FOPID controller design for the unstable magnetic ball suspension system. Eng. Sci. Technol. an Int. J. 24, 469–479. https://doi.org/10.1016/j.jestch.2020.08.001.

Dey, S., Banerjee, S., Dey, J., 2021. Design and Performance Analysis of Optimized Fractional Order PID Controller for Magnetic Levitation System. In: in: 2021

IEEE 4th International Conference on Computing, Power and Communication Technologies (GUCON). IEEE, pp. 1–6. https://doi.org/10.1109/GUCON50781.2021.9574026.

Ekinci, S., Izci, D., Hekimoglu, B., 2020. Henry Gas Solubility Optimization Algorithm Based FOPID Controller Design for Automatic Voltage Regulator. In: in: 2020 International Conference on Electrical, Communication, and Computer Engineering (ICECCE). IEEE, pp. 1–6. https://doi.org/10.1109/ICECCE49384.2020.9179406.

Ekinci, S., Izci, D., Kayri, M., 2021. An Effective Controller Design Approach for Magnetic Levitation System Using Novel Improved Manta-Ray Foraging Optimization. Arab. J. Sci. Eng.. https://doi.org/10.1007/s13369-021-06321-z.

García-Gutiérrez, G., Arcos-Aviles, D., Carrera, E.V., Guinjoan, F., Motoasca, E., Ayala, P., Ibarra, A., 2019. Fuzzy Logic Controller Parameter Optimization Using Metaheuristic Cuckoo Search Algorithm for a Magnetic Levitation System. Appl. Sci. 9, 2458. https://doi.org/10.3390/app9122458.

George, M.A., Kamat, D.V., Kurian, C.P., 2022. Electric vehicle speed tracking control using ANFIS based fractional order PID controller. J. King Saud Univ. - Eng. Sci.. https://doi.org/10.1016/j.jksues.2022.01.001.

Golnaraghi, F., Kuo, B.C., 2017. Automatic control systems. McGraw-Hill Education, London.

Gupta, S., Deep, K., Heidari, A.A., Moayedi, H., Wang, M., 2020. Opposition-based learning Harris hawks optimization with advanced transition rules: principles and analysis. Expert Syst. Appl. 158,. https://doi.org/10.1016/j.eswa.2020.113510 113510.

Heidari, A.A., Mirjalili, S., Faris, H., Aljarah, I., Mafarja, M., Chen, H., 2019. Harris hawks optimization: Algorithm and applications. Futur. Gener. Comput. Syst. 97, 849–872. https://doi.org/10.1016/j.future.2019.02.028.

Izci, D., Ekinci, S., 2021. An Efficient FOPID Controller Design for Vehicle Cruise Control System Using HHO Algorithm. In: in: 2021 3rd International Congress on Human-Computer Interaction, Optimization and Robotic Applications (HORA). IEEE, pp. 1–5. https://doi.org/10.1109/HORA52670.2021.9461336.

Izci, D., Ekinci, S., Eker, E., Dundar, A., 2021. Assessment of Slime Mould Algorithm Based Real PID Plus Second-order Derivative Controller for Magnetic Levitation System. In: in: 2021 5th International Symposium on Multidisciplinary Studies and Innovative Technologies (ISMSIT). IEEE, pp. 6–10. https://doi.org/10.1109/ISMSIT52890.2021.9604620.

Izci, D., Ekinci, S., Eker, E., Kayri, M., 2020. Improved Manta Ray Foraging Optimization Using Opposition-based Learning for Optimization Problems. In: in: 2020 International Congress on Human-Computer Interaction, Optimization and Robotic Applications (HORA). IEEE, pp. 1–6. https://doi.org/10.1109/HORA49412.2020.9152925.

Izci, D., Ekinci, S., Hekimoğlu, B., 2022a. A novel modified Lévy flight distribution algorithm to tune proportional, integral, derivative and acceleration controller on buck converter system. Trans. Inst. Meas. Control 44, 393–409. https://doi.org/10.1177/01423312211036591.

Izci, D., Ekinci, S., Zeynelgil, H.L., Hedley, J., 2022b. Performance evaluation of a novel improved slime mould algorithm for direct current motor and automatic voltage regulator systems. Trans. Inst. Meas. Control 44, 435–456. https://doi.org/10.1177/01423312211037967.

Izci, D., Hekimoğlu, B., Ekinci, S., 2022c. A new artificial ecosystem-based optimization integrated with Nelder-Mead method for PID controller design of buck converter. Alexandria Eng. J. 61, 2030–2044. https://doi.org/10.1016/j.aej.2021.07.037.

Kommula, B.N., Kota, V.R., 2020. Direct instantaneous torque control of Brushless DC motor using firefly Algorithm based fractional order PID controller. J. King Saud Univ. - Eng. Sci. 32, 133–140. https://doi.org/10.1016/j.jksues.2018.04.007.

Long, W., Jiao, J., Liang, X., Cai, S., Xu, M., 2019. A Random Opposition-Based Learning Grey Wolf Optimizer. IEEE Access 7, 113810–113825. https://doi.org/10.1109/ACCESS.2019.2934994.

Mirjalili, S., Lewis, A., 2016. The Whale Optimization Algorithm. Adv. Eng. Softw. 95, 51–67. https://doi.org/10.1016/j.advengsoft.2016.01.008.

Mirjalili, S., Mirjalili, S.M., Lewis, A., 2014. Grey Wolf Optimizer. Adv. Eng. Softw. 69, 46–61. https://doi.org/10.1016/j.advengsoft.2013.12.007.

Mughees, A., Mohsin, S.A., 2020. Design and Control of Magnetic Levitation System by Optimizing Fractional Order PID Controller Using Ant Colony Optimization Algorithm. IEEE Access 8, 116704–116723. https://doi.org/10.1109/ACCESS.2020.3004025.

Roy, P., Borah, M., Majhi, L., Singh, N., 2016. Design and implementation of FOPID controllers by PSO, GSA and PSOGSA for MagLev system, in: 2015 International Symposium on Advanced Computing and Communication, ISACC 2015. pp. 10–15. 10.1109/ISACC.2015.7377307..

Sadek, U., Sarjaš, A., Chowdhury, A., Svečko, R., 2017. Improved adaptive fuzzy backstepping control of a magnetic levitation system based on Symbiotic Organism Search. Appl. Soft Comput. 56, 19–33. https://doi.org/10.1016/j.asoc.2017.02.032.

Sharma, A., Sharma, A., Dasgotra, A., Jately, V., Ram, M., Rajput, S., Averbukh, M., Azzopardi, B., 2021. Opposition-Based Tunicate Swarm Algorithm for Parameter Optimization of Solar Cells. IEEE Access 9, 125590–125602. https://doi.org/10.1109/ACCESS.2021.3110849.

Sharma, T.K., Pant, M., 2018. Opposition-Based Learning Embedded Shuffled Frog-Leaping Algorithm, in: Pant, M., Ray, K., Sharma, Tarun K, Rawat, S., Bandyopadhyay, A. (Eds.), . Springer Singapore, Singapore, pp. 853–861. 10.1007/978-981-10-5687-1_76..

Tizhoosh, H.R., 2005. Opposition-Based Learning: A New Scheme for Machine Intelligence, in: International Conference on Computational Intelligence for Modelling, Control and Automation and International Conference on Intelligent Agents, Web Technologies and Internet Commerce (CIMCA-IAWTIC'06). IEEE, pp. 695–701. 10.1109/CIMCA.2005.1631345..

Yadav, S., Verma, S.K., Nagar, S.K., 2016. Optimized PID Controller for Magnetic Levitation System. IFAC-PapersOnLine 49, 778–782. https://doi.org/10.1016/j.ifacol.2016.03.151.

Yang, Y., Chen, H., Heidari, A.A., Gandomi, A.H., 2021. Hunger games search: Visions, conception, implementation, deep analysis, perspectives, and towards performance shifts. Expert Syst. Appl. 177,. https://doi.org/10.1016/j.eswa.2021.114864 114864.

Zhang, C.-L., Wu, X.-Z., Xu, J., 2021. Particle Swarm Sliding Mode-Fuzzy PID Control Based on Maglev System. IEEE Access 9, 96337–96344. https://doi.org/10.1109/ACCESS.2021.3095490.